Available online at www.sciencedirect.com
ScienceDirect
ELSEVIER
Palaeogeography, Palaeoclimatology, Palaeoecology 250 (2007) 1 – 17
PALAEO
www.elsevier.com/locate/palaeo

Stalagmite evidence from Belize indicating significant droughts at the time of Preclassic Abandonment, the Maya Hiatus, and the Classic Maya collapse

James W. Webster [a], George A. Brook [b,*], L. Bruce Railsback [c], Hai Cheng [d], R. Lawrence Edwards [d], Clark Alexander [e], Philip P. Reeder [f]

[a] *United States Environmental Protection Agency, Atlanta, Georgia, 30303, USA*
[b] *Department of Geography, University of Georgia, Athens GA 30602, USA*
[c] *Department of Geology, University of Georgia, Athens GA 30602, USA*
[d] *Department of Geology and Geophysics, University of Minnesota, Minneapolis MN 55455, USA*
[e] *Skidaway Institute for Oceanography, 10 Ocean Science Circle, Savannah GA 31411, USA*
[f] *Department of Geography, University of South Florida, Tampa FL 33620, USA*

Received 28 June 2006; received in revised form 10 January 2007; accepted 26 February 2007

Abstract

Paleoenvironmental data from a stalagmite from western Belize provide a 3300-year record of droughts that impacted the Maya civilization at least four times across a span of 1500 years, and the most sustained period of drought coincided with the collapse of Classic Maya civilization. The stalagmite, which comes from Macal Chasm in the Vaca Plateau, provides reliably dated reflectance, color, luminescence, and C and O stable isotope records for the period from 1225 B.C. to the present. The record thus encompasses the Maya Preclassic, Classic, and Postclassic periods. The Maya civilization peaked in population density and socioeconomic complexity during the Classic period extending from A.D. 25 to 900, but it declined abruptly over the years from A.D. 750 and 900. The stalagmite record indicates that a series of droughts, which collectively form the most prolonged dry interval in the 3300-year record, lasted from A.D. 700 to 1135 and thus coincided with the collapse of the Maya civilization. In addition, two earlier droughts evident in the stalagmite record coincided with the Preclassic Abandonment and the Maya Hiatus, two earlier declines in Maya civilization. A drought in the mid-1400s recorded in post-Classic documents is also evident in the stalagmite record. Collectively, these findings illustrate the dependence of Mayan civilization on water supplies and the impact of declining water resources on a vibrant civilization.

Keywords: Classic Maya collapse; Belize; Stalagmites; Drought; Caves; Paleoclimates

1. Introduction

The history of the Maya civilization in Mesoamerica is divided into two periods, the Preclassic and Classic periods. The Early Preclassic period began in the

* Corresponding author. Tel.: +1 706 542 2322; fax: +1 706 542 2388.
E-mail address: gabrook@uga.edu (G.A. Brook).

0031-0182/$ - see front matter © 2007 Elsevier B.V. All rights reserved.
doi:10.1016/j.palaeo.2007.02.022

Second Millennium B.C. and reached a pinnacle in northern Belize during the Late Preclassic period from 300 B.C. to A.D. 240. During the Classic period, from about A.D. 250 to A.D. 900, the Maya constructed impressive architecture, erected carved stone monuments (stelae), and developed a complex socioeconomic system (Chase and Chase, 1985). By A.D. 700 the Maya Lowlands supported larger numbers of people than existed anywhere else in Mesoamerica (Thompson, 1966; Adams and Jones, 1981).

Although the Maya civilization flourished for over one thousand years (Schele and Freidel, 1990), archaeological evidence suggests that the culture suffered a number of setbacks or declines of various severity and duration. During an event known as the Preclassic Abandonment period, probably from A.D. 150 to 200, there was urban abandonment, a drop in population, or a hiatus in construction at a number of Maya centers. Also, from A.D. 534 to 593 there was a sharp reduction in the dedication of stelae and monuments in Petén, the Mayan heartland in northern Guatemala (Fig. 1). This interval, known as the Maya Hiatus, is designated as the break between the Early and Late Classic periods. Both the Preclassic Abandonment and the Maya Hiatus proved to be temporary, if serious, setbacks.

The Classic Maya civilization collapsed permanently between A.D. 750 and 900. The first sign of collapse was a reduction in dedications of monuments and stelae

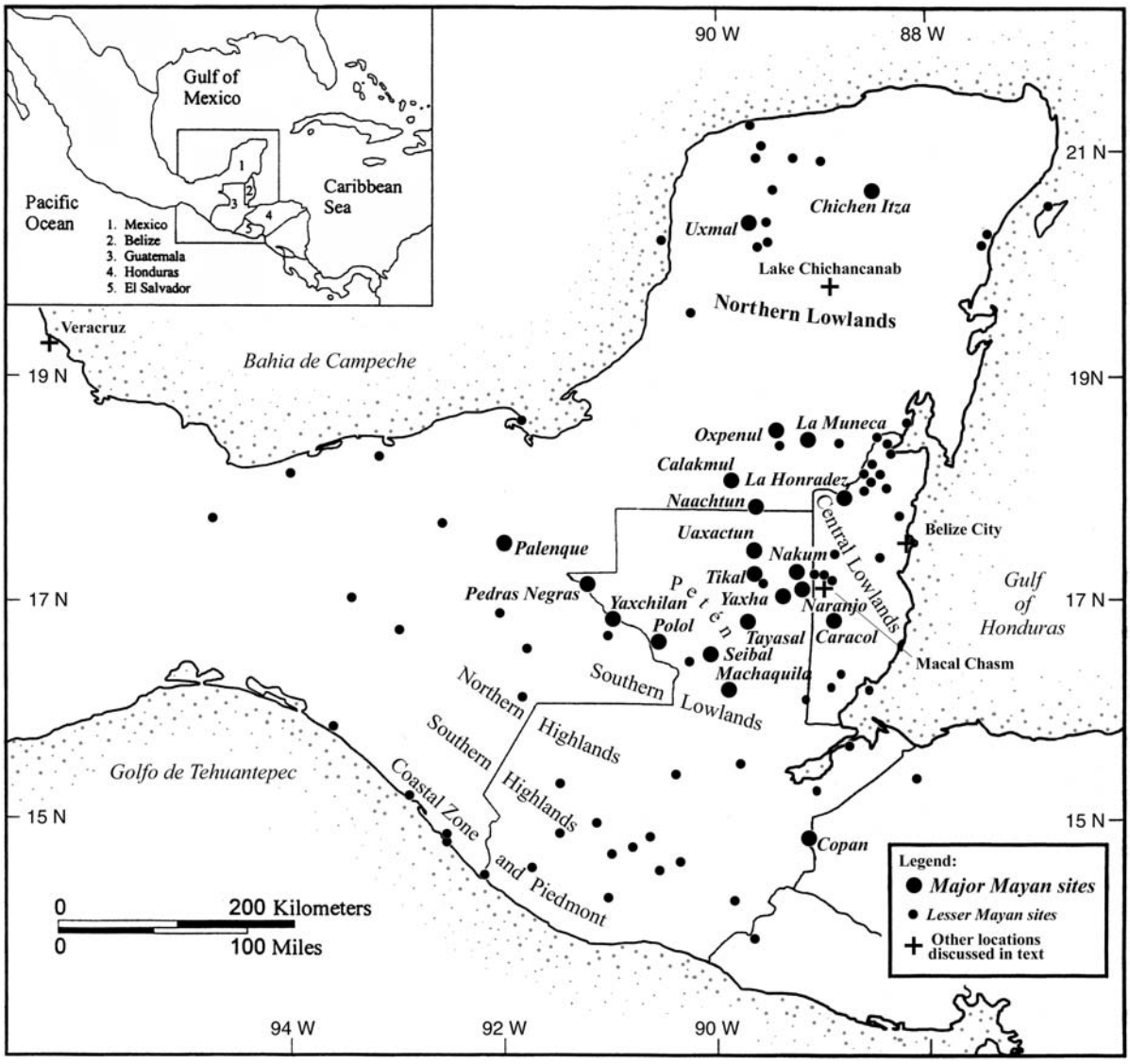

Fig. 1. Location map showing Macal Chasm and other important sites mentioned in the text.

after A.D. 790. The decline was well underway by A.D. 830 (Culbert, 1973). The end of the Classic period coincides with the last known recorded hieroglyphic date of A.D. 906. When Europeans arrived in the New World, much of the Petén was deserted. The pattern of the last inscribed dates at Maya sites indicates a slight southwest to northeast trend in the collapse sequence (Lowe, 1985).

Gill (2000) suggests three distinct phases for the Classic Maya collapse. Phase I (A.D. 760–810) led to initial abandonment of the western lowlands, where groundwater is scarce and rainfall was the primary source of water for Mayan cities. Phase II (A.D. 811–860) was characterized by abandonment of the southeastern lowlands, a region where freshwater lagoons provided at least some surface water supplies. Finally, Phase III (A.D. 861–910) led to large-scale abandonment of remaining cities in the central lowlands and in the north.

Availability and management of water greatly influenced human settlement in the Maya Lowlands (Scarborough and Gallopin, 1991) and much of Maya social innovation was centered on storing excess water for times of need (Schele and Freidel, 1990). In northern Yucatan the permanent water table is sufficiently shallow that it can be accessed by natural wells known as cenotes (Fig. 1). However, over much of the Maya Lowlands, the water table is too deep to have been available to the Maya. In response, they constructed artificial reservoirs to trap runoff (Schele and Freidel, 1990). For example, Gallopin (1990) estimates that the reservoirs at Tikal could have provided for the domestic needs of about 9600 people for a period of 6 to 18 months. Even with elaborate water capture and management systems, the Maya were greatly dependent upon adequate rainfall over much of their empire and were thus susceptible to frequent or prolonged droughts that approached or exceeded the capacity of their reservoirs. In fact, evidence of droughts in the region based on studies of lake and shallow ocean sediments has led many researchers to suspect that climate was responsible for the Classic Maya collapse (Hodell et al., 1995; Curtis et al., 1996; deMenocal, 2001; Rosenmeier et al., 2002; Haug et al., 2003).

This paper presents stalagmite data from Macal Chasm, a cave in Belize that adds to the growing body of evidence for major droughts in the Maya Lowlands at the time of the Maya collapse. In addition, it presents evidence that other periods of setback or decline in the Maya civilization were also caused by droughts not apparent in other records. Speleothems from caves in Belize have been shown to provide paleoenvironmental records of sea level (Dill et al., 1998) and El-Niño events (Frappier et al., 2002), and speleothems from elsewhere in Central America have been used as paleoclimate records (Lachniet et al., 2004a,b). An important aspect of the stalagmite record reported here is that it is accurately dated by ICPMS U-series and ^{210}Pb methods. Radiometric and AMS ^{14}C ages help to confirm the U-series and ^{210}Pb chronology used.

2. Study area

The climate of Belize, on the eastern coast of Mesoamerica, is dominated by the shifting northeast Trade winds and winter storms or “Northers”. Mean annual rainfall varies from about 1500 mm in the north to more than 4000 mm in the south. There is a distinct dry season that extends from about January to May. Temperatures range from ~10 to 35 °C.

The cave known as Macal Chasm is located on the Vaca Plateau west of the Rio Macal, in the Cavo District of Belize near the border with Guatemala (Fig. 1). The cave lies within the Central Lowlands area of the Maya region and about 60 km southeast of Tikal, a large Maya site in the Petén province of northern Guatemala. The site is also 15 km north of Caracol, the largest Maya site in Belize, and only 50 m from the ceremonial center of Ix Chel, a moderate-sized Maya settlement (Reeder et al., 1998; Webster, 2000). The cave is about 520 masl and receives approximately 1500 mm of rain annually (Walker, 1973). Cretaceous Campur Formation limestones, containing thin beds of dolomite, shale and siltstone, underlie the area (Vinson, 1962).

The entrance to Macal Chasm is a vertical shaft 5 m in diameter and 40 m deep that opens into the ceiling of a large chamber 62×45 m wide and 20 m high (Fig. 2). The cave, which is 155 m long, has two additional horizontal passage levels at 75 m and 90 m below the surface. Temperature in the chamber from which stalagmite MC01 was removed ranged from 18.5 to 21.5 °C during March 1996, 1997, and 1998 and averaged 21 °C. Relative humidity varied from 93% to 94% (Webster, 2000). Temperatures in the cave in March were typically 6–9 °C lower than temperatures at the surface above the cave.

3. Methods

An active stalagmite designated MC01 was removed from the entrance chamber of Macal Chasm, about 8 m southwest of the vertical entrance shaft (Fig. 2). The stalagmite, which is 92 cm long, was chosen because its location near the cave entrance rendered it susceptible to environmental conditions outside the cave.

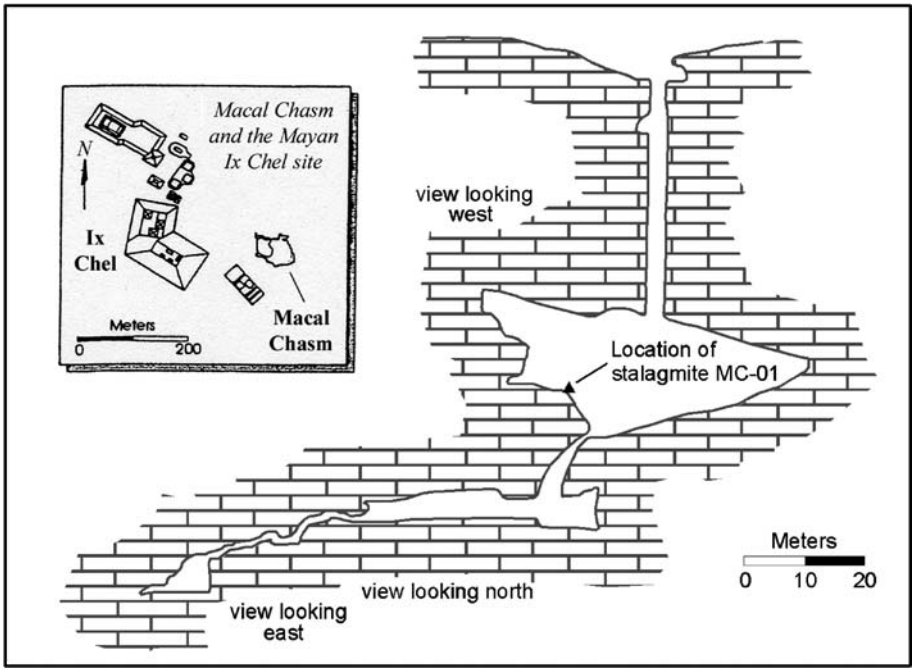

Fig. 2. Cross-section of Macal Chasm showing the location of stalagmite MC01.

The stalagmite was cut in half along the growth axis. One half was imaged for gray-scale and luminescence analysis and then was archived. Samples were taken from the other half for radiocarbon, U-series and ^{210}Pb dating, for stable O and C isotope analysis, and for preparation of thin sections for petrographic study.

Samples for radiometric and AMS radiocarbon dating were taken 1.3, 1.9, 4.8, 10.5, 35.5, 48 and 90.5 cm from the top of the stalagmite. Ages were corrected to a δ^{13}C of −25‰ (PDB). The percentage of old carbon in samples with both U-series and radiocarbon ages was estimated by varying the percent old carbon at 1% intervals from 0 to 20% and calibrating using OxCAL v. 3 (Ramsay, 1994, 1995) until the calibrated radiocarbon age matched the corresponding U-series ages discussed below. The same procedure was used to estimate the percentage of old carbon in samples at 1.3 and 1.9 cm dated by both the radiocarbon and ^{210}Pb methods.

Stalagmite carbonate for U-series dating was dissolved and spiked with a mixed ^{229}Th–^{233}U–^{236}U tracer (Cheng et al., 2000). Uranium and thorium were separated using anion exchange techniques similar to ones described by Edwards et al. (1987). The uranium and thorium isotopic compositions were then determined on a magnetic sector inductively coupled plasma mass spectrometer (Finnigan Element) using the multiplier in ion-counting mode (Shen et al., 2002). Ages were calculated (Table 1) using half-lives determined or reported in Cheng et al. (2000).

Three samples were taken from the upper 2 cm of the stalagmite for ^{210}Pb dating. ^{210}Pb is a naturally occurring radionuclide (half-life = 22.3 years) produced by the decay of its gaseous parent ^{222}Rn. Groundwaters absorb ^{222}Rn from soils as they migrate downwards and drip from the cave ceiling. ^{222}Rn is also absorbed from the air in the cave, providing an additional source for excess Pb-210 (Tanakara et al., 1998). The long-lived daughter isotope ^{210}Pb quickly ingrows (in less than a month) from ^{222}Rn in stalactites and stalagmites. ^{210}Pb accumulation rates in our stalagmite were calculated by producing profiles of excess ^{210}Pb activity with depth. Decrease in activity results from the decay of excess ^{210}Pb, and the slope of the regression through the excess ^{210}Pb data is mathematically related to the sediment accumulation rate. ^{210}Pb activities were determined using alpha spectrometry following the technique outlined by Nittrouer et al. (1979), which examines the activity of ^{210}Po, the granddaughter of ^{210}Pb. The carbonate is dissolved in HCl to which a ^{208}Po spike is added for yield determination. The Po isotopes are subsequently spontaneously electroplated onto silver planchets. Baskaran and Iliffe (1993) and Tanakara et al. (1998) have shown that there is a negligible supported ^{210}Pb signal in non-hydrothermally derived speleothem deposits, and thus the measured total ^{210}Pb activity is equal to the excess ^{210}Pb activity. The samples yielded an excess ^{210}Pb activity of 4.17±0.81 dpm/g for the uppermost sample, decreasing to 0.47±0.31 dpm/g in the deepest sample.

Table 1
ICPMS U-series age data for the Macal Chasm stalagmite where errors are 2σ

Sample ID	^{238}U (ppb)	^{232}Th (ppt)	^{230}Th/^{232}Th (atomic $\times 10^{-6}$)	δ^{234}U (measured)	^{230}Th/^{238}U (activity)	^{230}Th age ($\pm 2\sigma$) (uncorrected)	^{230}Th age ($\pm 2\sigma$) (corrected)
MC01-1.9 [a]	79.4±0.3	2984±30	9.3±0.5	988±13	0.0211±0.0010	1164±58	310±220
MC01-4.8 [a]	86.3±0.1	1658±13	14.6±0.6	1012±4	0.0170±0.0007	928±39	500±115
MC01-8.5 [a]	74.5±0.1	534±20	35.8±2.7	1124±6	0.0156±0.0010	802±51	650±65
MC01-10.5A	80.5±0.1	9440±80	9.4±0.2	1084±4	0.0666±0.0013	3537±70	985±640
MC01-10.5B	82.9±0.2	3040±30	13.4±0.2	1080±7	0.0297±0.0005	1570±26	775±400
MC01-10.5C [a]	126.6±1.2	321±11	104±6	1096±6	0.0160±0.0007	834±34	780±37
MC01-17.6A	56.4±0.2	20000±90	7.8±0.3	946±15	0.1670±0.0062	9733±386	1280±2100
MC01-17.6B [a]	53.6±0.1	1856±26	17.6±0.8	946±10	0.0369±0.0015	2088±86	1280±220
MC01-17.6C	53.5±0.2	7060±30	9.1±0.2	968±11	0.0731±0.0020	4119±116	1070±760
MC01-31.5 [a]	50.4±0.2	3758±30	18.0±0.5	972±10	0.0814±0.0020	4591±115	2890±440
MC01-40.25	52.7±0.1	13330±80	9.6±0.2	1019±5	0.1467±0.0031	8190±180	2450±1420
MC01-48 [a]	42.7±0.1	1760±20	25.9±0.7	616±8	0.0647±0.0015	4450±110	3300±310
MC01-90.5 [a]	56.2±0.1	1056±14	77.3±1.5	744±8	0.0879±0.0012	5629±85	5150±150

$\lambda_{230}=9.1577\times10^{-6}$/year, $\lambda_{234}=2.8263\times10^{-6}$/year, $\lambda_{238}=1.55125\times10^{10}$/year.
Corrected ^{230}Th ages assume an initial ^{230}Th/^{232}Th atomic ratio of $6.8\pm1.7\times10^{-6}$. This value was obtained by assuming that samples MC01-10.5B and C are of the same age and had the same initial ^{230}Th/^{232}Th ratio. Errors are arbitrarily assumed to be 25%. The upper limit is consistent with the constraint of measured ^{230}Th/^{232}Th ratio (8.1).

[a] Dates with lower uncertainties were used for the growth model. The numbers after the sample ID prefix MC01 show the distance (mm) from top of the stalagmite.

Variation in reflectance along the central growth axis was documented by scanning the cut surface on a standard flatbed scanner at 150 dpi and 8-bit gray level resolution. Gray level variation of reflected light was measured using digital image analysis software along a 2 mm wide (11 pixels) traverse along the central growth axis. Gray level (0 = black; 255 = white) varied from 133 to 255.

Luminescence was induced by illuminating the cut surface of the stalagmite with long wave ultraviolet light (320–420 nm) in a darkroom. Luminescence was recorded with a 35 mm camera fitted with Kodak Wratten Gelatin Filter #2E to prevent transmission of the excitation energy band. Photographic images were scanned and variations in luminescence (color) along a 2 mm wide (11 pixels) traverse down the central growth axis were documented using an image analysis software.

Variation in color along the growth axis exposed on the cut surface of the stalagmite was characterized by comparison to an indexed color scale. In this scale (Fig. 3), "1" corresponds to the most translucent calcite, which has a moderately dark gray color because light is adsorbed within the stalagmite rather than reflected. "2" and "3" correspond to less translucent calcite that is a light gray to light gray-tan. "4" through "8" correspond to colors from light tan to moderately dark brown imparted by increasing concentrations of fine-grained detrital material, as observed in thin-section. Quantitatively, these variations in color are demonstrated by an increase in brightness from 1 to 4 and a decrease from 5 to 8, with red barely dominant over green and blue in colors 1 to 4 but increasingly dominant in 5 to 8 (Fig. 3).

Carbonate samples for isotope analysis were taken at 0.5 cm intervals along the central growth axis and along a single growth layer 54 cm from the top of the stalagmite using a carbide dental burr. Carbonate powders were reacted under vacuum with 100% orthophosphoric acid at 50 °C following McCrea (1950) and Al-Aasm et al. (1990). Conventional cryogenic methods were used to

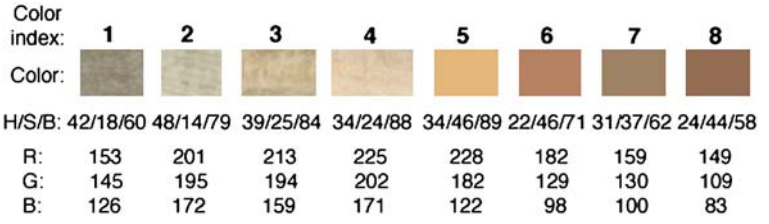

Fig. 3. Scale for measurement of color index shown in Fig. 5 and discussed in text. "H/S/B" indicates hue, saturation, and brightness of color; "R", "G", and "B" indicate red, green, and blue. (For interpretation of the references to colour in this figure legend, the reader is referred to the web version of this article.)

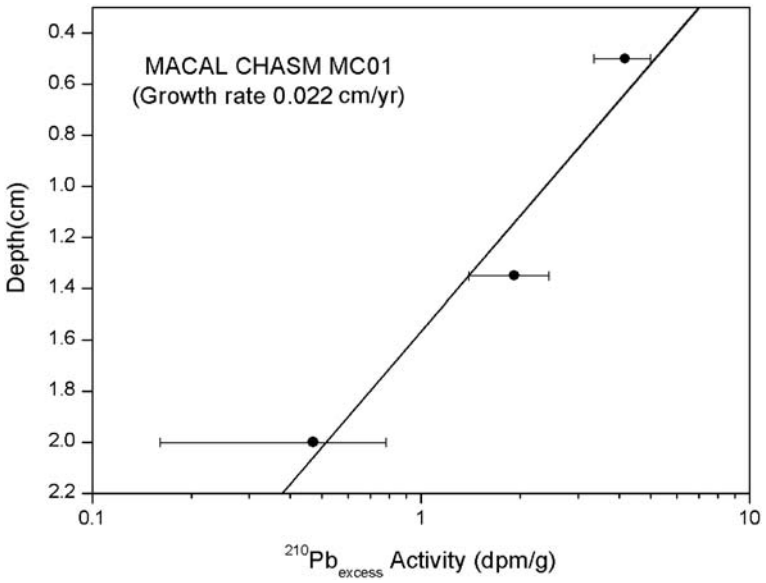

Fig. 4. Variations in the activity of excess ^{210}Pb with depth in the upper 2 cm of the stalagmite.

collect the evolved CO_2 for analysis on a Finnigan Delta E stable isotope ratio mass spectrometer.

4. Results

4.1. Chronology

Analysis of ^{210}Pb of three samples in the upper 2 cm of the stalagmite yielded a depositional rate of 0.022 cm/year and shows that MC01 was active when collected (Fig. 4)). Because the upper surface of MC01 dates to 1995/96, carbonate at 2 cm from the top of the stalagmite can be interpreted to be about 90 years old.

The 13 ICPMS U-series ages range from 310± 220 years at 1.9 cm to 5150±150 years at 90.5 cm (Table 1). ^{232}Th varied considerably in the samples, including the three samples from 10.5 cm depth and the three from 17.6 cm depth. Variations at 10.5 and 17.6 cm were used to estimate the correction for ^{230}Th contamination in all of the samples dated. Samples with

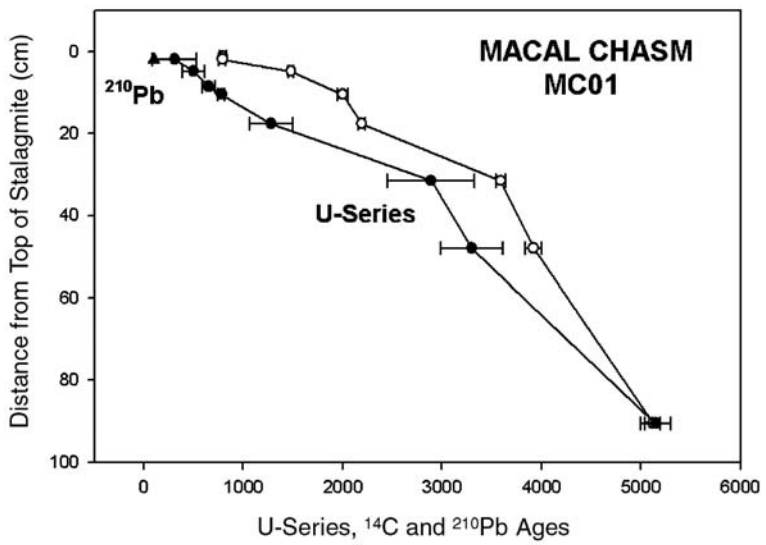

Fig. 5. ICPMS U-series and ^{210}Pb chronology for stalagmite MC01 compared with radiocarbon ages in ^{14}C years BP. Assuming the U-series and ^{210}Pb ages are correct old carbon in the stalagmite carbonate is estimated at 86–92%.

substantial ^{232}Th were not used in developing the MC01 chronology. In addition, sample MC01-1.9 (1.9 cm depth) with an age of 310±220 years was not used because of the large uncertainty. Instead we used our ^{210}Pb results indicating a calendar age of ~90 years at 2 cm depth. The resulting chronology is shown in Fig. 5. Ages for isotope, luminescence, color, and reflectance data were obtained by linear interpolation.

Seven samples were dated by both the radiocarbon (5 AMS, 2 radiometric) and U-series methods. By assuming that the U-series ages are accurate, we were able to estimate the percentage of old carbon in the stalagmite carbonate (Table 2). In addition, we used ^{210}Pb estimates of age at 1.3 and 1.9 cm to determine the percentage of old carbon in radiocarbon-dated samples from these locations. The percentage modern carbon estimated by comparison with U-series ages varied from 86 to 92%. The percentage of modern carbon based on the ^{210}Pb age estimates was 91% at both 1.3 and 1.9 cm. We did not use the radiocarbon ages in developing a chronology for the Belize stalagmite, but their consistency with the ^{210}Pb and U-series ages (regardless of corrections) supports the chronology used.

4.2. Petrography

Petrographic analysis and X-ray diffraction show that the stalagmite is calcite. The stalagmite consists mostly of dense translucent calcite with lesser zones of porous calcite (Fig. 6A and B). Material insoluble in HCl averaged 0.5% in two samples of porous calcite, whereas one sample of dense translucent calcite contained no insoluble residue. Carbon and nitrogen analysis of the residue yielded 6.3% C and 0.7% N, and elemental analysis showed that K, P, and Zn are present, suggesting the presence of finely divided organic matter, organic acids, charcoal, and possibly even guano. X-ray diffraction revealed the presence of the clay minerals vermiculite, kaolinite and chlorite, as well as quartz and iron oxides.

Detritus-rich layers mostly contain particles too small for resolution in a light microscope (i.e., clay-sized particles), and the largest particles within such layers are 0.20 mm in size and thus can be classified as silt. This fine detrital material is usually in distinct layers between clearer layers of nearly pure calcite. These layers thin or become less distinct toward the central growth axis of the stalagmite and thus the crest of any one layer (Fig. 6C and D). A very few larger grains, up to 0.14 mm in size and thus in the range of fine sand, are present in the layers of clear calcite but not in the detritus-rich layers. These larger grains typically consist of red-brown fine minerals, the color of which suggests the presence of Fe oxides like those found in tropical soils.

The presence of fine detrital material between distinct calcite layers suggests deposition of that fine material as an aerosol during the dry part of some years, when drip water

Table 2
Radiocarbon age data for the Macal Chasm stalagmite

Depth in cm (A = AMS)	Sample ID	Laboratory ID[a]	δ^{13}C ‰ with respect to PDB	^{14}C age (years BP±1σ)[b]	Modern carbon (%)[c]	Calibrated age (cal. years A.D. or B.C.)	Calibrated age (calendar years before present)
1.3 A	MCAMS-1	NSRL-11465	−11.3	795±35	91/Pb	1860–1920 A.D.	110
1.9 A	MCAMS-2	NSRL-11466	−7.7	790±35	91/Pb	1810–1920 A.D.	135
4.8 A	MCAMS-3	NSRL-11467	−12.4	1480±30	88/U	1400–1520 A.D.	540
10.5	MC01-10.5	UGA-7416	−11.3	2000±50	86/U	1160–1300 A.D.	770
17.65 A	MCAMS-4	NSRL-11468	−8.8	2190±35	90/U	620–780 A.D.	1300
31.5	MC01-31.5	UGA-7417	−10.6	3590±50	90/U	1000–800 B.C.	2900
48.0 A	MC01-48	AZ-UGA-7396	−10.4	3920±80	90/U	1430–1250 B.C.	3340
90.45 A	MC01-90.45	AZ-UGA-7394	−10.2	5120±80	92/U	3340–3000 B.C.	5170

[a] Radiometric dating was carried out at the Center for Applied Isotope Analysis (CAIS), University of Georgia (UGA). Two samples were dated at the NSF-University of Arizona AMS laboratory after pretreatment and preparation at CAIS. Four samples were dated at the National Ocean Sciences AMS facility (NOSAMS), Woods Hole Oceanographic Institution. These were pretreated and prepared at the University of Colorado at Boulder INSTAAR Laboratory for AMS Radiocarbon Preparation and Research (NSRL).

[b] Age corrected to δ^{13}C of −25‰.

[c] Modern carbon estimated by comparing the U-series (U) or ^{210}Pb (Pb) age with the radiocarbon age.

failed to wash dust off the surface of the stalagmite. Thinning of these layers near the central growth axis is compatible with their origin as a dusty aerosol, in that drip water on the crest of the stalagmite washed away the dust there that remained elsewhere on the surface of the stalagmite. The location of stalagmite MC01 near the

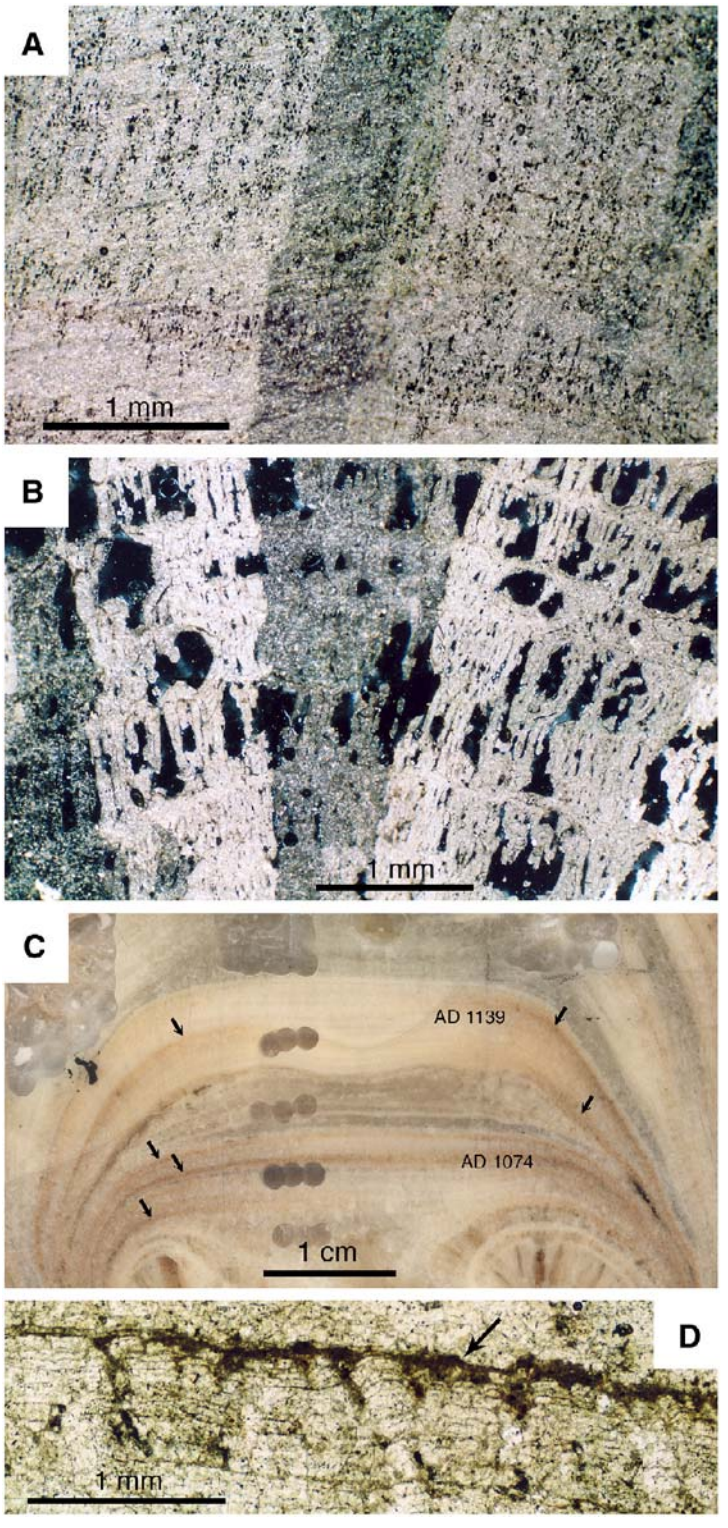

entrance of Macal Chasm probably made deposition of such dust in dry periods more likely than it would have been farther into the cave, and it may have favored evaporation of incoming water in dry periods before such water could drip onto the stalagmite, further favoring preservation of dust on the stalagmite surface. In contrast to the fine detritus, the presence of a few coarser grains in layers of clearer calcite suggests that such grains were washed in by drip water during wetter periods when any dust was washed away by the drip water. We therefore infer that the brown zones rich in fine detritus formed during drier periods when drip rates slowed or nearly stopped. By contrast, the dense, translucent calcite with just a few larger detrital grains probably formed under wetter conditions when the stalagmite received a continuous flow of dripping water and underwent uninterrupted growth.

4.3. Luminescence, color, and reflectance

Luminescence in stalagmites is produced by organic acids and so is related to productivity in the soil and vegetation cover above the cave (Shopov et al., 1994). At Macal Chasm plant growth is rarely limited by temperature, and so luminescence can be expected to function as a proxy for availability of moisture, as was suggested in the classic work of Baker et al. (1998, their Fig. 1). Luminescence in stalagmite MC01 varies greatly, generally with longer periods of greater luminescence punctuated by briefer intervals of lesser luminescence (Fig. 7). The most sustained interval of lesser luminescence, and interval with the smallest value of luminescence, is the period encompassing and postdating the collapse of Classic Maya civilization (Fig. 8D).

Color of the stalagmite, as recorded relative to the color index shown in Fig. 3, is closely correlative with luminescence (Fig. 8E). Values of color index less than 4 correlate with greater luminescence, whereas greater values of the color index correlate with lesser luminescence. The two parameters thus agree in their indication of relative dryness, in that low values of the color index, which are indicative of translucent calcite that appears to have formed under a continuous flow of water that kept the stalagmite tip free of dust, correspond to greater values of luminescence suggestive of greater moisture above the cave. On the other hand, greater values of color index, which are indicative of the presence of fine detritus that seemingly accumulated when flow of water was inadequate to keep the tip of the stalagmite free of dust, correlate with lesser luminescence suggestive of less moisture above the cave.

Reflectance shows a less pronounced correlation with luminescence and color (Fig. 8F). For example, lesser reflectance correlates with lower values of the color index and more luminescence in the period from about A.D. 1150 to A.D. 1460. However, in general the correlation is not strong, largely because both clear translucent calcite and darker brown detritus-rich calcite reflect little light but represent very different environmental conditions (and thus correspond to different levels of luminescence).

4.4. Oxygen and carbon isotopes

Along the central growth axis of MC01, $\delta^{18}O$ and $\delta^{13}C$ values range from −7‰ to −2.5‰ (PDB) and −14‰ to −6‰ (PDB) respectively (Fig. 8A and B). A strong correlation ($R^2=0.87$) between $\delta^{18}O$ and $\delta^{13}C$ along a single growth layer (Fig. 9A) indicates that kinetic effects such as evaporation and rapid degassing of CO_2 influenced the isotopic composition of the stalagmite, rather than equilibrium fractionation alone (Hendy, 1971). In fact, on either side of the growth axis there is a noticeable increase in both $\delta^{18}O$ and $\delta^{13}C$ of about 1‰ and 2‰ respectively (Fig. 9B). The location of the stalagmite near the cave entrance probably enhanced both evaporation and degassing. Thus variation of $\delta^{18}O$ through the stalagmite is likely to be at least in part a record of the extent of evaporation and thus of dryness of climate, wherein any increase in evaporation with drier climate would have led to greater $\delta^{18}O$ of stalagmite calcite.

In addition to kinetic controls such as evaporation and degassing, $\delta^{18}O$ values of stalagmite carbonate are influenced by temperature at deposition ($\delta^{18}O_{CaCO3}$ increases with lower temperature) and by the $\delta^{18}O$ of the

Fig. 6. Detailed images of stalagmite MC01 from Macal Chasm, Belize. A. Photomicrograph in cross-polarized transmitted light of relatively non-porous calcite of which most of the stalagmite consists. Parts of three vertically elongate crystals are shown; the one in the middle is photographed with least bright birefringence. B. Photomicrograph in cross-polarized transmitted light of porous calcite in stalagmite. Parts of six vertically elongate crystals are shown, each with differing brightness of birefringence; black areas are porosity. C. Scanned image of a small part of the cut surface of the stalagmite, centered on the growth axis 11 to 14 cm from the top of the stalagmite. "AD 1074" and "AD 1139" indicate age estimates shown in Fig. 8. Arrows point to brown layers of very fine (clay-sized) detrital material; note that layers are less pronounced near the center of the image and thus along the growth axis. Sets of three holes at mid-left and holes at upper left are sampling sites for dating and stable isotope analysis. D. Photomicrograph in plane-polarized transmitted light showing layer of fine detrital material (dark layer at arrow) to which date of A.D. 1074 has been assigned. Note lesser concentration of detrital material to left, which is toward the center of stalagmite. (For interpretation of the references to colour in this figure legend, the reader is referred to the web version of this article.)

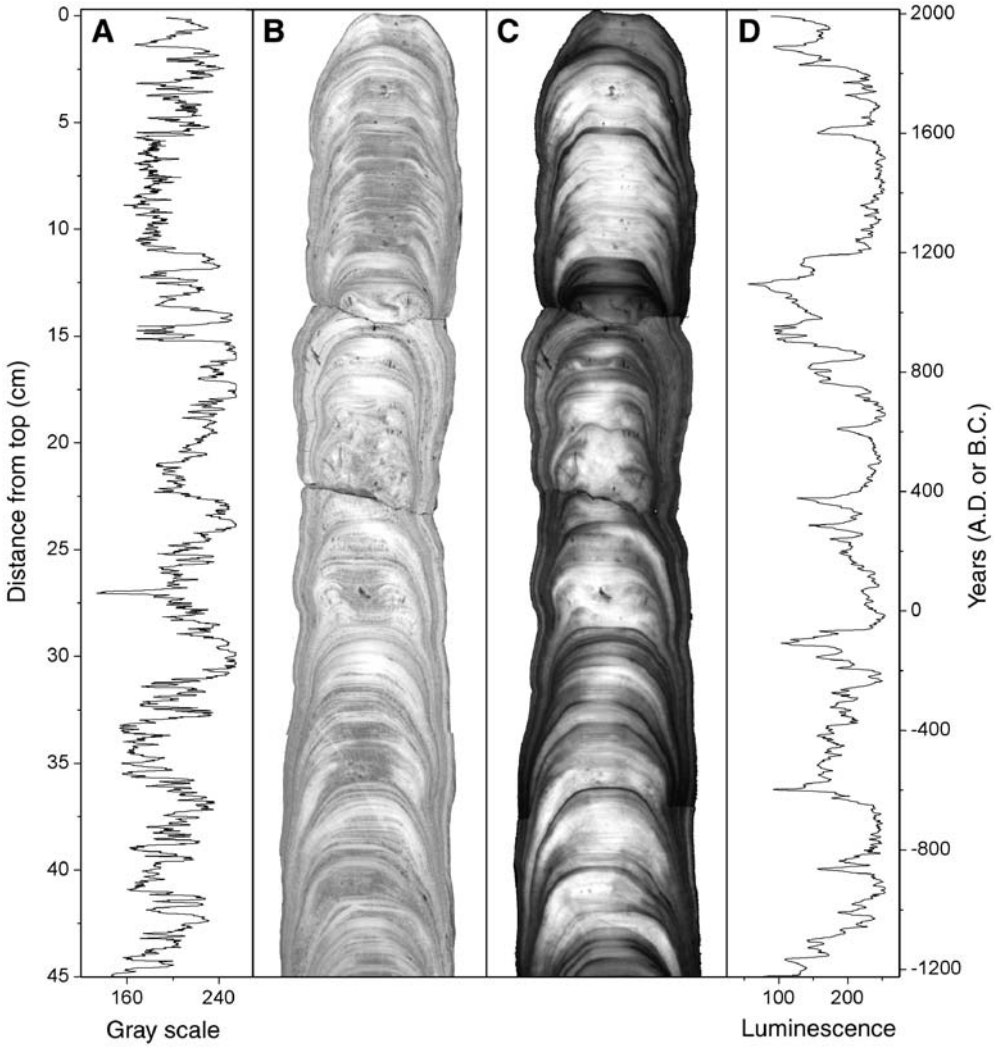

Fig. 7. Variations in gray color and luminescence in the MC01 stalagmite. Digital gray-level images of visible color (B) and UV-stimulated luminescence (C) in the upper 45 cm of MC01. Variations in gray color (A) and luminescence (D) along the central growth axis.

precipitating dripwaters ($\delta^{18}O_w$). There are no published isotope data for rainfall in Belize. However, incomplete monthly data for 1962 to 1985 (IAEA, 129 monthly values) for Veracruz on the Gulf of Mexico coast of Mexico (~500 km west–northwest of Macal Chasm across the Yucatan Peninsula) indicate that lower $\delta^{18}O_w$ is associated with greater monthly rainfall ($R^2=0.26$) and greater temperature ($R^2=0.18$) (Fig. 10A). Similar correlations of lesser $\delta^{18}O_w$ with greater rainfall have been observed in Panama (Lachniet and Patterson, 2006) and elsewhere around the world (Araguas-Araguas et al., 1998; Gonfiantini et al., 2001; Njitchoua et al., 1999; Rietti-Shati et al., 2000; Vuille and Werner, 2005). Moreover, the Veracruz data show that at high temperatures of between 26 °C and 29 °C there is a 12‰ range in $\delta^{18}O$, further suggesting that $\delta^{18}O_w$ of rainfall at the height of the summer wet season is more dependent on rainfall amount than on temperature (Fig. 10B). The relationships in Veracruz rainfall suggest that more negative $\delta^{18}O_{CaCO3}$ values of MC01 stalagmite carbonate would indicate increased monthly rainfall during the wet season, and possibly slightly warmer temperatures. This relationship combines fortuitously with the kinetic effects discussed above, in that greater rainfall characterized by lower $\delta^{18}O_w$ values would allow less evaporation and thus lower values of stalagmite $\delta^{18}O_{CaCO3}$, whereas less rainfall characterized by greater $\delta^{18}O_w$ values would allow more evaporation and a further increase in $\delta^{18}O_{CaCO3}$.

$\delta^{13}C$ of stalagmite carbonate is determined by the $\delta^{13}C$ of the carbon dioxide in the soil above the cave and

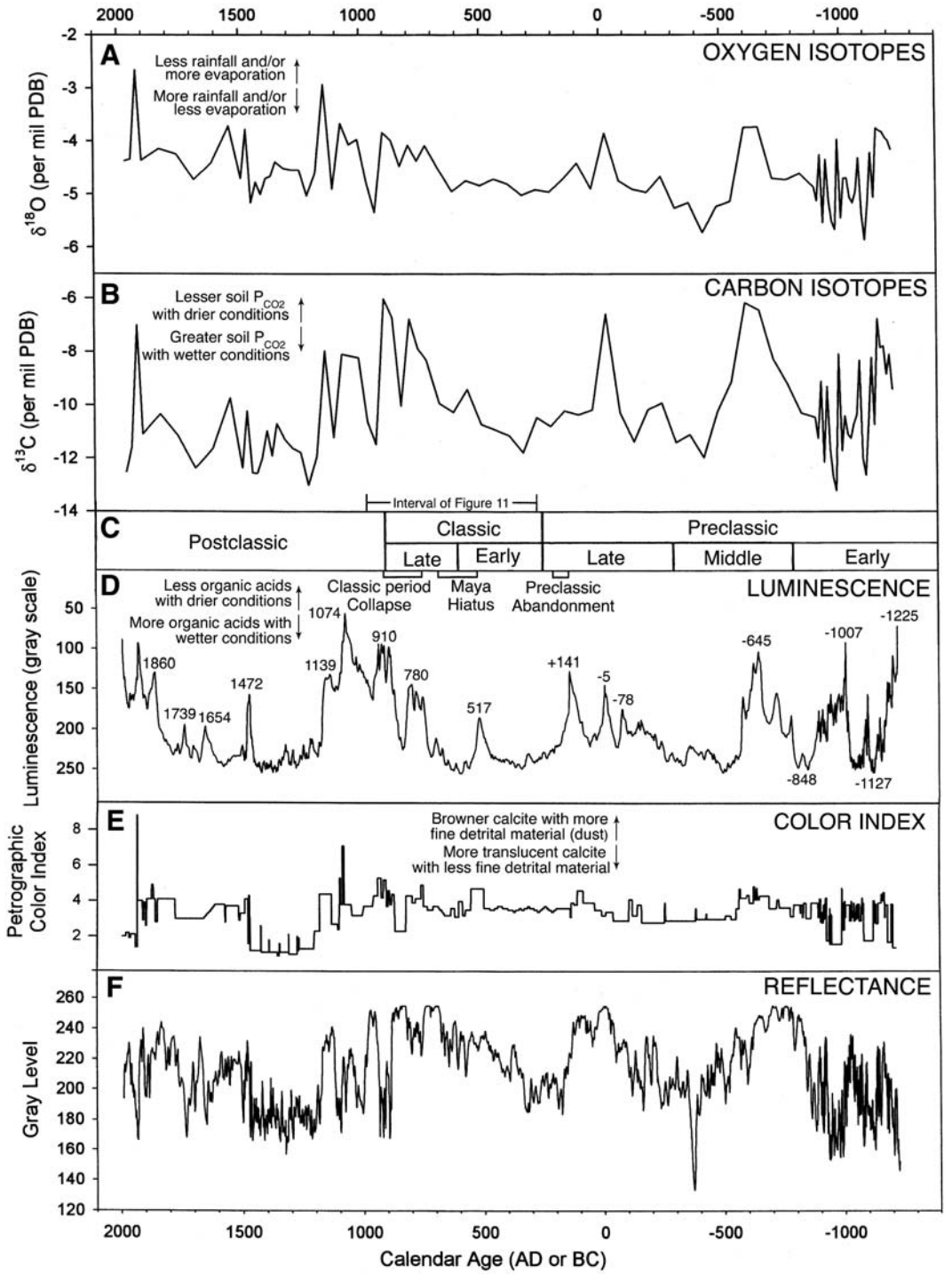

Fig. 8. Stable isotope, luminescence, color, and reflectance records from stalagmite MC01 compared with Maya cultural periods. All five records are plotted so that interpreted indicators of dryer conditions are upward and interpreted indicators of wetter conditions are downward.

by the degree to which open system dissolution of limestone occurs, as well as by the extent of degassing. Where the plant cover is largely the C_3 vegetation typical of wetter climates, $\delta^{13}C$ can be expected to be lower than if the plant cover is predominantly the C_4 vegetation of hotter drier climates (Brook, 1999). During dry conditions with reduced plant growth, less soil CO_2 can be expected in percolating waters, and

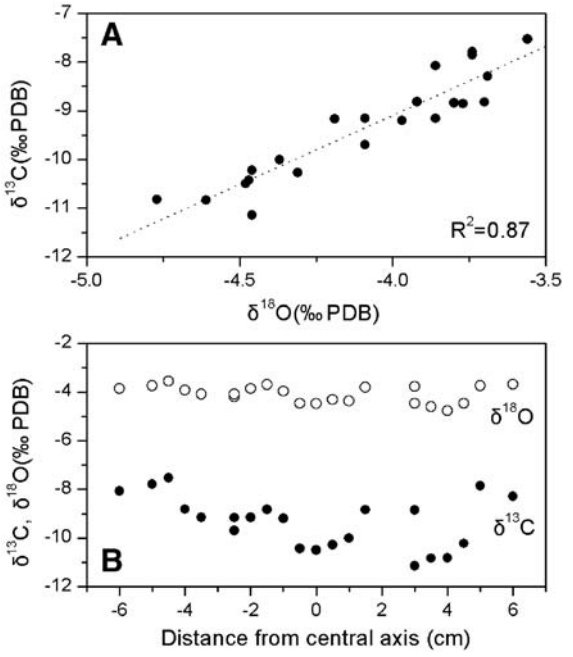

Fig. 9. Comparison of $\delta^{18}O$ and $\delta^{13}C$ along a single growth layer of stalagmite MC01 (A), and variations with distance from the central growth axis (B).

therefore less exchange of soil carbon with carbon derived from the limestone.

Low levels of soil CO_2 would limit C exchange in the soil zone, causing $\delta^{13}C$ to increase also. Thus wetter conditions at Macal Chasm should bring lower $\delta^{13}C_{CaCO3}$ because of higher levels of soil CO_2. Under closed-system conditions the percentage of dissolved C in percolating waters that is derived from the host rock increases as soil PCO_2 decreases (Hendy, 1971). At Macal Chasm, upland soils are relatively thin and infiltration rates during intense rains are high. Because MC01 lies >50 m below the surface, it is likely that some dissolution of carbonate occurs under closed-system conditions. Therefore, in dry years the $\delta^{13}C$ of dripwaters, and of carbonate precipitated on MC01, should increase because of lesser soil PCO_2. In wet years the opposite should be the case due to higher soil PCO_2 as a result of increased plant growth and root respiration. This logic is corroborated by the observation by Frumkin et al. (2000) of greater $\delta^{13}C$ of spelean carbonate deposited in dry periods and lesser $\delta^{13}C$ carbonate deposited in wetter periods in a stalagmite from Israel.

5. The MC01 paleoclimate record and the Maya collapse

The results discussed above suggest that color, luminescence, $\delta^{18}O_{CaCO3}$ and $\delta^{13}C_{CaCO3}$ values of stalagmite MC01 should serve as proxies for paleoenvironmental conditions above Macal Chasm, with browner colors, lesser luminescence, and increased $\delta^{18}O$ and $\delta^{13}C$ indicative of drier and possibly cooler conditions. The four records indeed correlate to show similar, but not identical, variations (Fig. 8). One reason for the differences between records is difference in resolution. The luminescence and reflectance data have a spatial resolution of ~0.18 mm, whereas the isotope data are spaced at 5 mm intervals and have a sample resolution of 2 mm (the diameter of the drill bit). Because growth rates estimated from ^{210}Pb and U-series ages range from 0.069 to 0.402 mm/year, the isotope data therefore have a temporal resolution of ~5–30 years at ~10–70 year intervals, and the color and luminescence data have a resolution of 0.5–3 years. Because of sharp peaks and higher resolution of the luminescence data, we consider the luminescence record to be the best tool in estimating the timing of wet and dry intervals on the Vaca Plateau above Macal Chasm.

Marked variations in all four variables along the stalagmite indicate frequent and abrupt changes in climate at Macal Chasm during the last 3300 years, which are represented by the upper 45 cm of MC01. For example, the Early Preclassic was a time of fluctuating climate, with major droughts at 1225 and 1007 B.C. that ended after ~848 B.C. as the climate became significantly wetter (Fig. 8). The Early–Middle Preclassic boundary is marked by a sharp increase in $\delta^{18}O$ and $\delta^{13}C$, as well as whiter carbonate with lower luminescence, marking the beginning of much drier conditions. These lasted through the first half of the Middle Preclassic and peaked at ~645 B.C. The rest of the Middle Preclassic and the first half of the Late Preclassic (~550–100 B.C.) experienced moist conditions that allowed expansion of the Maya civilization. After 100 B.C. conditions became drier with a modest drought at 78 B.C. followed by more severe droughts at 5 B.C. and A.D. 141 (Fig. 8).

The major drought at A.D. 141 coincides with Preclassic Abandonment (Fig. 8). It is thus the first of a series of droughts coincident with declines in Mayan activity and population. The drought of A.D. 141 associated with Preclassic Abandonment marks the end of the Preclassic and the beginning of the Early Classic Period, which saw a return to moister conditions.

A minimum in luminescence and thus an apparent drought at about A.D. 517 coincides with the beginning of the Maya Hiatus. It is thus the second drought coincident with a major Mayan decline (see also Rosenmeier et al., 2002). The Maya Hiatus marks the end of the Early Classic period and the beginning of the Late

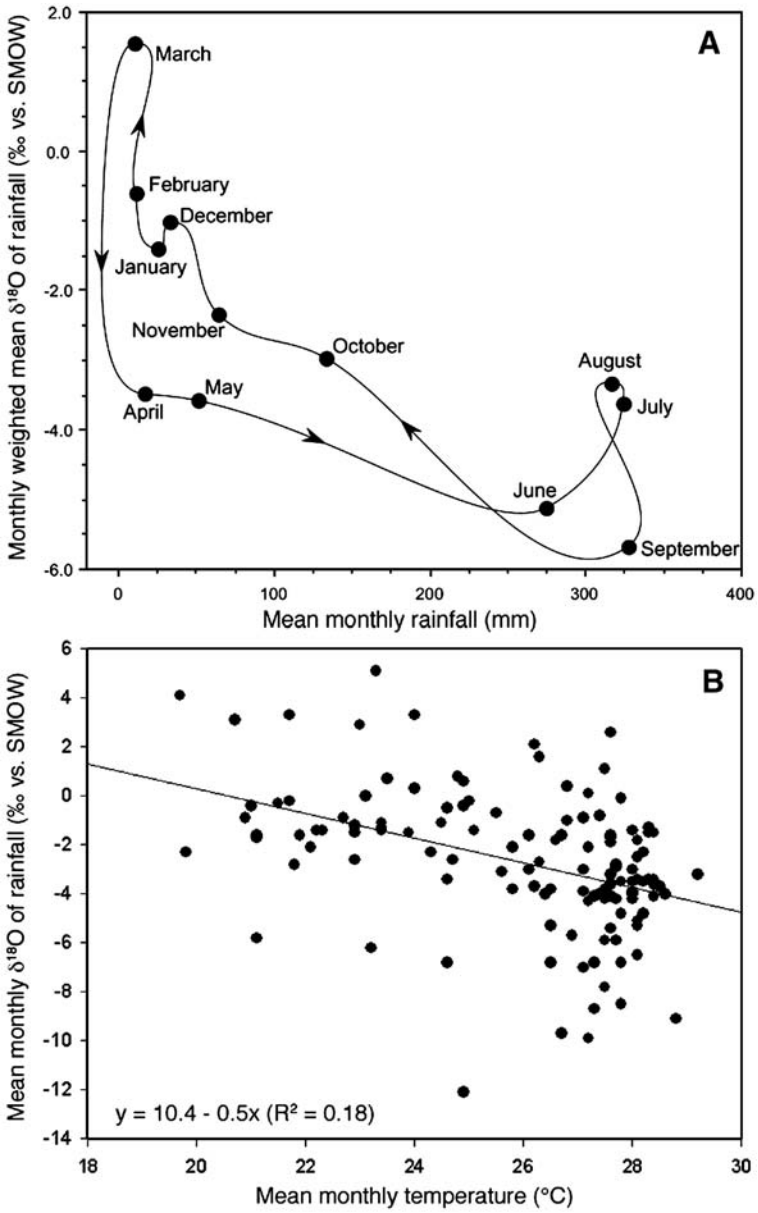

Fig. 10. A. Means of monthly $\delta^{18}O$ and amount of precipitation at Veracuz, Mexico. B. Mean $\delta^{18}O$ of rainfall and temperature at Veracruz, Mexico, for individual months in the period from 1962 to 1985. Data are from the International Atomic Energy Agency's (IAEA) GNIP/ISOHIS website at http://isohis.iaea.org/News.asp accessed 22 November 2006.

Classic. The Late Classic saw a return to warm, wet conditions until ~A.D. 750.

The wet conditions of the early Late Classic period gave way to a series of droughts centered at about A.D. 780, 910, 1074, and 1139. High $\delta^{13}C$ and $\delta^{18}O$ values combine with minima in luminescence to suggest the most extreme droughts in the entire 3300-year record from stalagmite MC01. The first two of these droughts coincide with the collapse of the Maya civilization (Fig. 8). The three separate phases of abandonment ending at A.D. 810, 860, and 910 identified by Gill (2000) match well with the data from the Belize stalagmite showing peak drought conditions at A.D. 754–798, 871, and 893–922, with successive droughts increasing in severity.

The sequence of events leading to the Classic Maya collapse has been examined by analyzing the number of sites engaged in producing monuments at any given time (Lowe, 1985). This approach uses the assumption that more monuments are dedicated during times of plenty and fewer at times of hardship. In fact, Lowe's (1985)

data show four periods when monument building leveled off, namely around A.D. 395, 550, 670, and 770. Within the uncertainties of our ages, these correspond well with the stalagmite evidence for drier conditions at A.D. 313, 517, 673–700, and 754–798 (Fig. 11). Furthermore, after peaking and leveling off around A.D. 750–790, monument building dropped off significantly before leveling off briefly at ~A.D. 860 when the stalagmite data show a brief return to wetter conditions ~A.D. 837. With the approach of an even more severe drought peaking initially at A.D. 893 monument building ceased entirely by A.D. 909.

The correlation of drier periods in the record from the Macal Chasm stalagmite with reported droughts extends later than the Maya Classic collapse. For example, the stalagmite's luminescence, color, and stable isotope data all suggest a generally wet period from about A.D. 1150 to A.D. 1840, but with a pronounced drought at A.D. 1472. Folan and Hyde (1985) comment on a period of drought, cold, and famine from A.D. 1441 to 1461 reported in the Maya Books of Chilam Balam of Chumayel and Mani, corresponding to the first of these droughts. The timing of that drought is again, within error, coincident with the drought seen in the stalagmite record. Finally, the stalagmite's luminescence, color, and stable isotope data all show that conditions became much drier after A.D. 1850 (Fig. 8).

The Macal Chasm stalagmite record indicates that the Central Lowlands of Belize were significantly drier during the Late Classic and Early Postclassic than at any time during the preceding 1200 years. In fact, the interval in our record from A.D. 750 to 1150 was the most prolonged dry phase in our 3300-year record. The Classic Maya collapse occurred at the end of the second of four major droughts one or two centuries apart, with each lasting several decades to one or two centuries. The length of the dry interval and the number of major droughts following one after the other are most likely the reasons that the Maya civilization was unable to survive. The water that fueled the growth of cities and agriculture during phases of abundant rainfall in the Early Classic and the first half of the Late Classic could no longer be relied upon. Decades of drought forced the population to abandon the cities and adjacent farmlands.

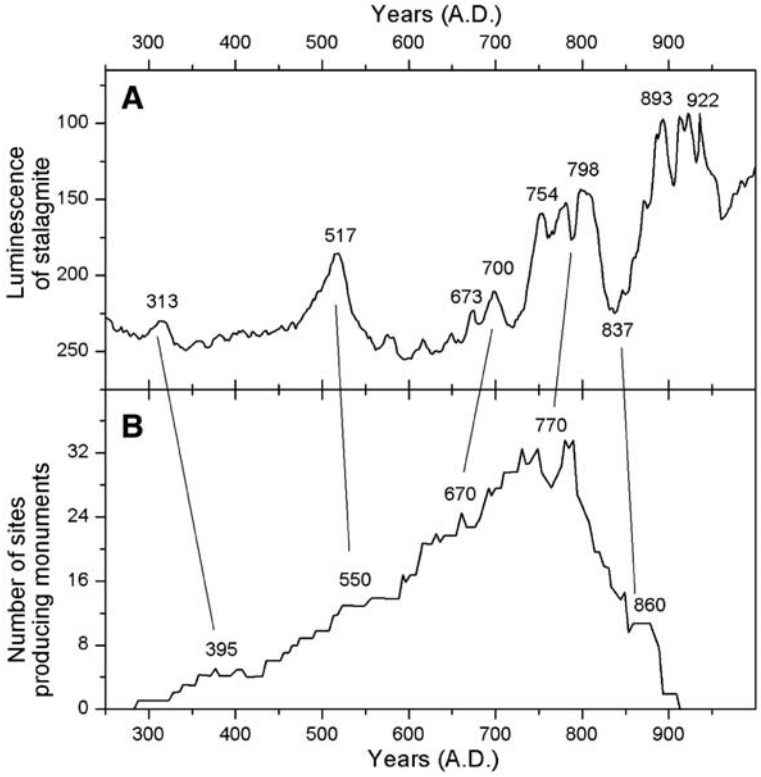

Fig. 11. Droughts in Belize indicated by a reduction in stalagmite MC01 luminescence compared with Maya monument production. Within the limitations of our dating accuracy, periods when monument production leveled off before peaking around A.D. 770 (B), correlate well with periods of low luminescence (A). The rapid decline in monument production after ca. A.D. 770 was halted temporarily at ca. A.D. 860 most likely because of the wetter conditions around A.D. 837 indicated by the luminescence record.

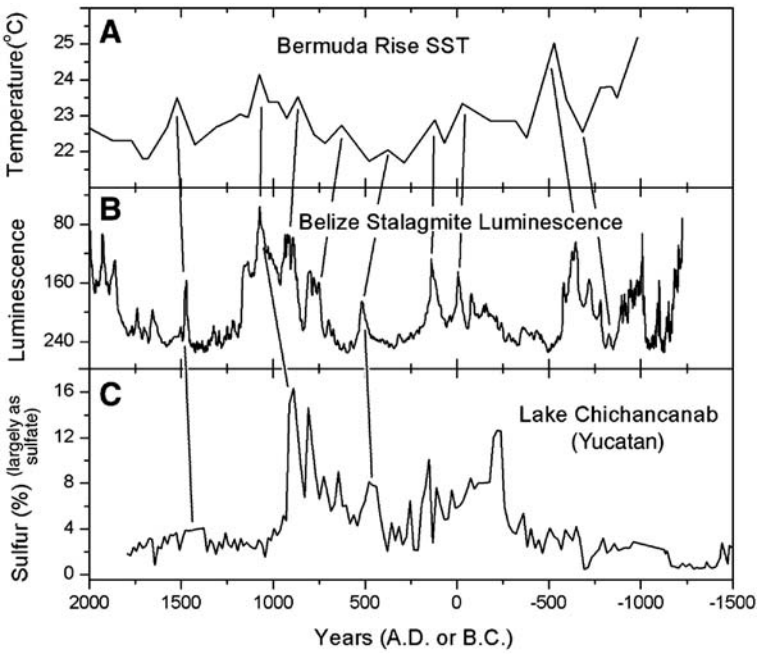

Fig. 12. Comparison of the Belize stalagmite record with Bermuda Rise and Lake Chichancanab data. A. Bermuda Rise BC-004 sea-surface temperatures (SST) (Keigwin, 1996). B. Luminescence in stalagmite MC01 from Macal Chasm, Belize (this study). C. Sulphur content of sediments in a core from Lake Chichancanab, Yucatan, Mexico (Hodell et al., 1995).

The droughts persisted for four centuries before rainfall returned to Early Classic levels. By then the people had adopted a very different survival strategy.

6. Comparison with other records

The record from the Macal Chasm stalagmite shows striking correlations with at least two other paleoenvironmental records. For example, lesser values of luminescence in the Macal Chasm stalagmite, interpreted above as indicators of dryness, correlate with highs in Bermuda Rise sea-surface temperature (SST) (Keigwin, 1996) (Fig. 12). Keigwin (1996) observed that variation in the Bermuda Rise record was correlative with climate change well beyond the Sargasso Sea and probably corresponded to climate change at a "basin or hemispheric scale". Lesser values of luminescence also correlate with greater concentrations of sulfur in sediments from Lake Chichancanab in Yucatan, Mexico over the last 2000 years (Hodell et al., 1995). Hodell et al. (1995) used greater sulfur concentrations as an indicator of drier conditions, so that the fluctuations of the Macal Chasm and Lake Chichancanab records are in agreement.

These correlations demonstrate that the Macal Chasm stalagmite provides a regional record of climate, rather than a local record of land-use change or a record only of changes within the cave itself. More significantly, they demonstrate that the dry periods in the Macal Chasm record were widespread events that would have affected the entire Mayan civilization.

7. Conclusions

The paleoclimate record from the Macal Chasm stalagmite includes luminescence, color, and stable isotopes that add to a growing body of evidence suggesting that severe dryness affected a broad region of Mesoamerica and contributed to the collapse of the Maya civilization during the Late Classic period. The high resolution of the record also allows recognition of droughts that induced Preclassic Abandonment and the Maya Hiatus in the centuries prior to the final drought-induced collapse. The stalagmite also records at least one drought that is mentioned in historical records centuries after the Classic collapse.

Acknowledgments

We thank Drs. Jaime Awe, John Morris, and Alan Moore of the Belize Institute of Archaeology for supporting our permit applications, and also Mr. William Reynolds, of the Lower Dover Field Station, and other members of the Northern Vaca Plateau Geoarchaeological Project (NVPGP) for field assistance and material support.

This research was supported by the National Science Foundation (NSF 9628765 and 9908415), the Geological Society of America, and the NVPGP. We thank Randy Culp of the CAIS at the University of Georgia for his assistance in calculating the percentage of old carbon in samples that were dated by the radiocarbon method.

References

Adams, R.E.W., Jones, R.C., 1981. Spatial patterns and regional growth among Classic Maya cities. American Antiquity 46, 301–322.

Al-Aasm, I.S., Taylor, B.E., South, B., 1990. Stable isotope analysis of multiple carbonate samples using selective acid extraction. Chemical Geology 80, 119–125.

Araguas-Araguas, L., Froehlich, K., Rozanski, K., 1998. Stable isotope composition of precipitation over southeast Asia. Journal of Geophysical Research, Atmospheres 103 (D22), 28721–28742.

Baker, A., Genty, D., Smart, P.L., 1998. High-resolution records of soil humification and paleoclimatic change from variations in speleothem luminescence excitation and emission wavelengths. Geology 26, 903–906.

Baskaran, M., Iliffe, T., 1993. Age determination of recent cave deposits using ^{210}Pb — a new technique. Geophysical Research Letters 20, 603–606.

Brook, G.A., 1999. Arid zone paleoenvironmental records from cave speleothems. In: Singhvi, A.K., Derbyshire, E. (Eds.), Paleoenvironmental Reconstruction in Arid Lands. Oxford & IBH Publishing Co. Pvt. Ltd., New Delhi, pp. 217–262.

Chase, A.F., Chase, D.Z., 1985. Postclassic temporal and spatial frames for the Lowland Maya: a background. In: Chase, A.F., Rice, P.M. (Eds.), The Lowland Maya Postclassic. University of Texas Press, Austin, pp. 9–22.

Cheng, H., Edwards, R.L., Hoff, J., Gallup, C.D., Richards, D.A., Asmerom, Y., 2000. The half-life of uranium-234 and thorium-230. Chemical Geology 169, 17–33.

Culbert, T.P., 1973. The Classic Maya Collapse. University of New Mexico Press, Albuquerque.

Curtis, J.H., Hodell, D.A., Brenner, M., 1996. Climate variability on the Yucatan Peninsula (Mexico) during the past 3500 years, and implications for Maya cultural evolution. Quaternary Research 46, 37–47.

deMenocal, P.B., 2001. Cultural responses to climate change during the late Holocene. Science 292, 667–673.

Dill, R.F., Land, L.S., Mack, L.E., Schwarcz, H.P., 1998. A submerged stalactite from Belize: petrography, geochemistry, and geochronology of massive marine cementation. Carbonates and Evaporites 13 (2), 189–197.

Edwards, R.L., Chen, J.H., Wasserburg, G.J., 1987. ^{238}U–^{234}U–^{230}Th–^{232}Th systematics and the precise measurement of time over the past 500,000 years. Earth and Planetary Science Letters 81, 175–192.

Folan, W.J., Hyde, B.H., 1985. Climatic forecasting and recording among the ancient and historic Maya: an ethnohistoric approach to epistemological and paleoclimatological patterning. In: Folan, W.J. (Ed.), Contributions to the Archaeology and Ethnohistory of Greater Mesoamerica. Southern Illinois University Press, Carbondale, pp. 15–48.

Frappier, A., Sahagian, D., González, L.A., Carpenter, S.J., 2002. El Niño events recorded by stalagmite carbon isotopes. Science 298, 565.

Frumkin, A., Ford, D.C., Schwarcz, H.P., 2000. Paleoclimate and vegetation of the last glacial cycles in Jerusalem from a speleothem record. Global Biogeochemical Cycles 14, 863–870.

Gallopin, G.G., 1990. Water Storage Technology at Tikal, Guatemala. M.S. Thesis, University of Cincinnati, Cincinnati.

Gill, R.B., 2000. The Great Maya Droughts: Water, Life and Death. University of New Mexico Press, Albuquerque, New Mexico.

Gonfiantini, R., Roche, M.A., Olivry, J.C., Fontes, J.C., Zuppi, G.M., 2001. The altitude effect on the isotopic composition of tropical rains. Chemical Geology 181 (1–4), 147–167.

Haug, G.H., Günther, D., Peterson, L.C., Sigman, D.M., Hughen, K.A., Aeschlimann, B., 2003. Climate and the collapse of Maya civilization. Science 299, 1731–1735.

Hendy, C., 1971. The isotopic geochemistry of speleothems I. The calculation of the effects of different modes of formation on the isotope composition of speleothems and their applicability as palaeoclimate indicators. Geochimica et Cosmochimica Acta 35, 801–824.

Hodell, D.A., Curtis, J.H., Brenner, M., 1995. Possible role of climate in the collapse of Classic Maya civilization. Nature 375, 391–394.

Keigwin, L.D., 1996. The little ice age and medieval warm period in the Sargasso Sea. Science 274, 1504–1508.

Lachniet, M.S., Patterson, W.P., 2006. Use of correlation and stepwise regression to evaluate physical controls on the stable isotope values of Panamanian rain and surface waters. Journal of Hydrology 324 (1–4), 115–140.

Lachniet, M.S., Asmerom, Y., Burns, S.J., Patterson, W.P., Polyak, V., Seltzer, G.O., 2004a. Tropical response to the 8200 yr B.P. cold event: speleothem isotopes indicate a weakened early Holocene monsoon in Costa Rica. Geology 32, 957–960.

Lachniet, M.S., Burns, S.J., Piperno, D.R., Asmerom, Y., Polyak, V.J., Moy, C.M., Christenson, K., 2004b. A 1500-year El Niño/southern oscillation and rainfall history for the Isthmus of Panama from speleothem calcite. Journal of Geophysical Research 109, D20117. doi:10.1029/2004JD004694.

Lowe, J.W.G., 1985. The Dynamics of Apocalypse: A Systems Simulation of the Classic Maya Collapse. University of New Mexico Press, Albuquerque, New Mexico.

McCrea, J.M., 1950. On the isotope chemistry of carbonates and a paleoclimatic scale. Journal of Chemical Physics 18, 849–857.

Nittrouer, C.A., Sternberg, R.W., Carpenter, R., Bennett, J.T., 1979. The use of ^{210}Pb geochronology as a sedimentological tool: application to the Washington continental shelf. Marine Geology 31, 297–316.

Njitchoua, R., Sigha-Nkamdjou, L., Dever, L., Marlin, C., Sighomnou, D., Nia, P., 1999. Variations of the stable isotopic compositions of rainfall events from the Cameroon rain forest, Central Africa. Journal of Hydrology 223 (1–2), 17–26.

Ramsay, C.B., 1994. Analysis of chronological information and radiocarbon calibration: the program OxCal. Archaeological Computing Newsletter 41, 11–16.

Ramsay, C.B., 1995. Radiocarbon calibration and analysis of stratigraphy: the OxCal program. Radiocarbon 37 (2), 425–430.

Reeder, P., Brady, J., Webster, J., 1998. Geoarchaeological investigations on the Northern Vaca Plateau, Belize. Mexicon 20 (2), 37–43.

Rietti-Shati, M., Yam, R., Karlen, W., Shemesh, A., 2000. Stable isotope composition of tropical high-altitude fresh-waters on Mt. Kenya, Equatorial East Africa. Chemical Geology 166 (3–4), 341–350.

Rosenmeier, M.F., Hodell, D.A., Brenner, M., Curtis, J.H., Guilderson, T.P., 2002. A 4000-year lacustrine record of environmental change in the southern Maya Lowlands, Petén, Guatemala. Quaternary Research 57, 183–190.

Scarborough, V.L., Gallopin, G.G., 1991. A water storage adaptation in the Maya Lowlands. Science 251, 658–662.

Schele, L., Freidel, D., 1990. A Forest of Kings. Quill William Morrow, New York.

Shen, C.-C., Edwards, R.L., Cheng, H., Dorale, J.A., Thomas, R.B., Moran, S.B., Weinstein, S., Edmonds, H.N., 2002. Uranium and thorium isotopic and concentration measurements by magnetic sector inductively coupled plasma mass spectrometry. Chemical Geology 185, 165–178.

Shopov, Y.Y., Ford, D.C., Schwarcz, H.P., 1994. Luminescent microbanding in speleothems: high-resolution chronology and paleoclimate. Geology 22, 407–410.

Tanakara, A., Taira, H., Yamakawa, K., 1998. Application of excess ^{210}Pb dating method to stalactites. Geochemical Journal 32, 183–187.

Thompson, J.E.S., 1966. The Rise and Fall of Maya Civilization, 2nd ed. University of Oklahoma Press, Norman.

Vinson, G.L., 1962. Upper Cretaceous and Tertiary stratigraphy in Guatemala. Bulletin of the American Association of Petroleum Geologists 46, 425–456.

Vuille, M., Werner, M., 2005. Stable isotopes in precipitation recording South American summer monsoon and ENSO variability: observations and model results. Climate Dynamics 25 (4), 401–413.

Walker, S.H., 1973. Summary of climate records for Belize. British Foreign and Commonwealth Office Overseas Development Administratio, Land Resources Division, Surbiton, Surrey, England.

Webster, J.W., 2000. Speleothem Evidence of Late Holocene Climate Variation in the Maya Lowlands of Belize, Central America, and Archaeological Implications. Ph.D. Dissertation, University of Georgia.